EFFECTS OF MULTIAXIAL LOADING ON CYCLIC PLASTICITY AND FATIGUE BEHAVIOUR OF AUSTENITIC STAINLESS STEEL (AISI 303)

L. Reis, A. Cabrita, B. Li and M. de Freitas

Dept. of Mech. Engineering
Instituto Superior Técnico
Av. Rovisco Pais, 1,
1049-001, Lisboa, Portugal
E-mail:
luís.g.reis@ist.utl.pt
bli@ist.utl.pt
mfreitas@dem.ist.utl.pt

ABSTRACT

Components and structures are usually under multiaxial loading conditions. Among several structural steels the austenitic stainless steels are widely used in various engineering applications, one of their main features is the strong corrosion resistance. Materials are usually submitted to complex loadings, which could cause micro-structural changes, affecting their physical and mechanical properties and consequently causing multiaxial fatigue damage.
The purposes of this work are to study the influence of the different multiaxial fatigue loading paths on fatigue life and crack orientation, comparing the test results with theoretical results from multiaxial fatigue models. Tests were carried out in load control for several multiaxial loading paths and then fractographic analyses of specimen fracture surface were carried out. Results show that the different multiaxial loading paths have a relevant preponderance on fatigue life and are determinant on the fatigue crack initial orientation, which is predicted by critical plane models.

KEY WORDS: Austenitic stainless steel, Multiaxial fatigue, Loading paths, Proportional and non-proportional loadings, Fatigue life prediction, Fractographic analysis.

1. INTRODUCTION

Mechanical components are generally submitted to complex fatigue loadings that generate multiaxial stress states in correspondent critical points. During the last forty years researchers have extensively investigated the problem of multiaxial fatigue assessment in order to provide engineers safe methods for the fatigue life prediction in the presence of complex stress states [1]. One recent inquiry had demonstrated that 70% of the companies have encountered with fatigue problems [2]. Stainless steels are present in many industries applications and therefore are submitted to multiaxial stress states. Austenitic stainless steels are ductile, tough and, most importantly, easy to form and weld. They have f.c.c. microstructure. There are numerous applications for this type of stainless steel, ranging from domestic kitchen thinks and building façades to commercial food processing equipment and chemical plant piping [3, 4].

In this study, several non-proportional multiaxial fatigue tests were carried out on *AISI 303* steel. The objective of these fatigue tests is to study the behavior of the material when subject to the multiaxial fatigue loading paths. To evaluate the shear stress amplitude two approaches were used, the *von Mises* equivalent stress, [5], and the MEC approach [6, 7]. Fatigue critical plane models, such as the Findley, the Fatemi-Socie, the SWT and the Liu criterions are used to analyse the potential crack plane orientation. The predictions given by these models are compared with experimental results.

2. MATERIAL DATA, SPECIMEN FORM AND TEST PROCEDURE

In this work, the material studied is the austenitic stainless steel *AISI 303*. The chemical composition is shown in Table 1. In order to characterize the cyclic stress-strain behavior of the material studied tension-compression low cycle fatigue tests were carried out, [8]. Monotonic and cyclic mechanical properties are shown in Table 2.

Table 1*- Chemical composition of the material studied – AISI 303 steel (in wt%) [5].*

AISI 303 Stainless steel	Chemical composition								
	C	Si	Mn	P	S	Cr	Ni	Mo	Cu
	0.12	1.00	2.00	0.060	0.25	18.00	9.00	---- -	--- --

In order to study the effects of the multiaxial loading paths and in particular both the axial and the torsional

component on the fatigue life, a series of loading paths were applied in the experiments as shown in Table 3. In Table 4 are shown the reference multiaxial fatigue loading paths. A biaxial servo hydraulic machine performed the tests of biaxial cyclic tension-compression with cyclic torsion. Test conditions were as follows: frequency 3-5 Hz at room temperature and laboratory air. Tests ended up when the specimens were completely broken or after a million cycles.

Table 2 *- Monotonic and cyclic mechanical properties of AISI 303 [5].*

Tensile strength	$R_m(MPa)$	625
Yield strength	$R_{p0.2,monotonic}(MPa)$	330
Elongation	$A(\%)$	58
Young's modulus	$E\ (GPa)$	178
Yield strength	$R_{p0.2,cyclic}(MPa)$	310
Strength coefficient	$K'\ (MPa)$	2450
Strain hardening exponent	n'	0.35
Fatigue strength coefficient	$\sigma'_f(MPa)$	534
Fatigue strength exponent	b	-0.07
Fatigue ductility coefficient	ε'_f	0.05
Fatigue ductility exponent	c	-0.29

The geometry and dimensions of the specimen are shown in Figure 1:

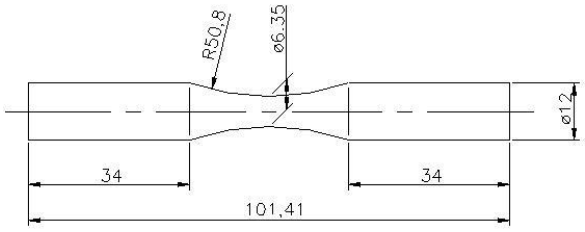

Figure 1 *- Specimen geometry for biaxial cyclic tension-compression with cyclic torsion tests [8].*

Table 3 *- Multiaxial fatigue loading paths.*

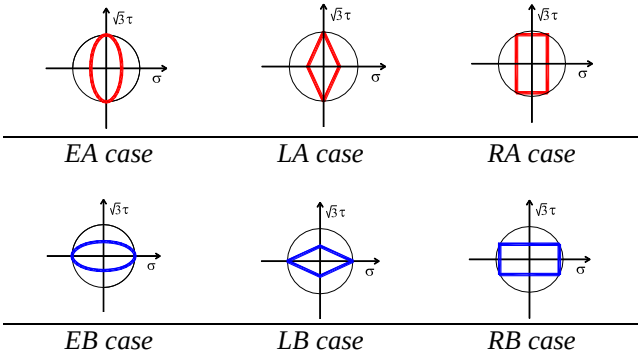

Table 4 *– Reference Multiaxial fatigue loading paths.*

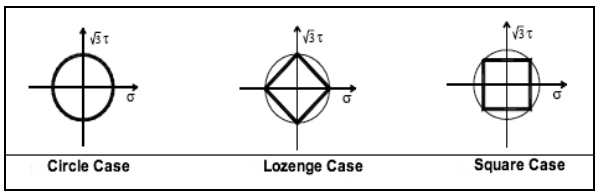

3. THEORETICAL ANALYSIS OF THE FATIGUE LIFE PREDICTION

Many multiaxial fatigue models have been proposed in the last decades [9] and some of them are applied in this work; the shear stress amplitude is one of the important parameters in the formulations of the multiaxial fatigue damage models.

3.1. von Mises approach

According to von Mises criterion [10], the shear stress occurs in a plane equally inclined to all the main directions. For x-y-z Cartesian system the *von Mises* equivalent stress can be written as equation (1):

$$\sigma_{eq}=\frac{1}{\sqrt{2}}\sqrt{(\sigma_x-\sigma_y)^2+(\sigma_y-\sigma_z)^2+(\sigma_x-\sigma_z)^2+6(\tau_{xy}^2+\tau_{yz}^2+\tau_{xz}^2)} \quad (1)$$

For biaxial loading of tension-compression with cyclic torsion the expression can be simplified, equation (2):

$$\sigma_{eq}=\sqrt{\sigma_x^2+3(\tau_{xy})^2} \quad (2)$$

3.2. MCE Approach for evaluating shear stress amplitude

From the stress invariant (Sine's criterion), which is express by the amplitude and the mean value of equivalent shear stress and by the hydrostatic stress, in which the equivalent shear stress amplitude is represented by the square root of the second invariant of the stress deviator, $\sqrt{J_{2,a}}$ [6], avoiding the search of critical plane, equation (3):

$$\sqrt{J_{2,a}}+\alpha(\sigma_{H,med})\leq\beta \quad (3)$$

where α and β are material constants. The innovation of this model is the $\sqrt{J_{2,a}}$ calculation. Whereas minimum circumscribed circle (MCC) approach [11] defines the shear stress amplitude as the radius of the minimum circle circumscribing to the loading path, minimum circumscribed ellipse (MCE) approach compute the effective shear stress amplitude taking into account the non-proportional loading effect. The load traces are represented and analyzed in the transformed deviatoric stress space, where each point represents a

value of $\sqrt{J_2}$ and the variations of $\sqrt{J_2}$ are shown during a loading cycle. The schematic representation of the MCE approach and the relation with MCC approach are illustrated in Figure 2:

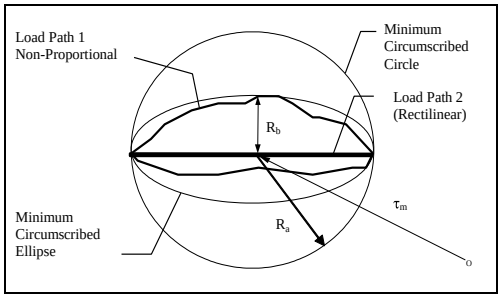

Figure 2 *- The MCC and MCE circumscribing to shear stress traces, Ra and Rb are the major and minor radius of MCE, respectively [6].*

The idea of the MCE approach is to construct a minimum circumscribed ellipse that can enclose the whole loading path throughout a loading block in the transformed deviatoric stress space. Rather than defining $\sqrt{J_{2,a}} = R_a$, by the MCC approach, in MCE approach R_a and R_b are the lengths of the major semi-axis and the minor semi-axis of the minimum circumscribed ellipse respectively. The ratio of R_b / R_a represents the non-proportionality of the shear stress path. The important advantage of this new MCE approach is that it can take into account the non-proportional loading effects in an easy way. As shown in Figure 2, for the non-proportional loading path 1, the shear stress amplitude is defined as, equation (4):

$$\sqrt{J_{2,a}} = \sqrt{R_a^2 + R_b^2} \tag{4}$$

For the proportional loading path 2, it is defined as $\sqrt{J_{2,a}} = R_a$ since R_b is equal to zero (rectilinear loading trace).

3.3. Critical Plane models

The ingredients of the critical plane criteria are the normal and shear stresses acting on a material plane Δ. The various proposed formulae are different, but the process to follow is merely the same. One must firstly, found the critical plane and secondly, check if the criterion is satisfied on this plane. If the criterion is not satisfied, then a fatigue crack may appear on the critical plane. Therefore, the orientation of the initiated crack coincides with the orientation of the critical plane [11].

Findley **criterion**
Findley [12] proposed a critical plane model, which predicts that the fatigue crack plane is the plane orientation θ with maximum *Findley* damage parameter, equation (5):

$$\max_{\theta}\left(\sigma_a + k\sigma_{a,\max}\right) \tag{5}$$

where τ_a is the shear stress amplitude on a plane θ, $\sigma_{n,\max}$ is the maximum normal stress on that plane θ and k is a material parameter $\left(k_{AISI303} = 0.2\right)$.

Brown-Miller **criterion**
Brown and *Miller* [13] proposed that the shear and normal strain on the plane of maximum shear must be considered. The simplified formulation of the theory for *case A* cracks is (equation (6):

$$\max_{\theta}\left(\frac{\Delta\gamma_{\max}}{2} + S\Delta\varepsilon_n\right) \tag{6}$$

Critical plane is the plane of maximum shear strain range $\Delta\gamma_{\max}$ with major value of normal strain range $\Delta\varepsilon_n$; S is the normal strain effects coefficient and is determined experimentally $\left(S_{AISI303} = 0.2\right)$.

Fatemi-Socie **criterion**
Fatemi-Socie [14] proposed a model that predicts the critical plane is the plane orientation θ with the maximum F-S damage parameter, equation (7):

$$\max_{\theta}\left[\frac{\Delta\gamma_{\max}}{2}\left(1 + k\frac{\sigma_{n,\max}}{\sigma_y}\right)\right] \tag{7}$$

where $\frac{\Delta\gamma_{\max}}{2}$ is the maximum shear strain amplitude on a plane θ, $\sigma_{n,\max}$ is the maximum normal stress on that plane, σ_y is the material monotonic yield strength and k is a material constant $\left(k_{AISI303} = 0.2\right)$.

S-W-T **criterion**
Smith, Watson and *Topper* [15] proposed a model that predicts that the fatigue crack plane is the plane orientation θ with maximum normal stress (the maximum principal stress), equation (8):

$$\max_{\theta}\left(\sigma_n \frac{\Delta\varepsilon_1}{2}\right) \tag{8}$$

where σ_n is the normal stress on a plane θ, $\Delta\varepsilon_1$ is the principal strain range on that plane.

Liu **criterion**
Liu [16] proposed an energy method to estimate the fatigue life, based on virtual strain energy (VSE). This

model considers two parameters associated with two different Modes of fatigue cracks, a tensile failure mode (Mode I), ΔW_I, and a shear failure mode (Mode II), ΔW_{II}. Failure is expected to occur on the plane θ in the material, having the maximum VSE quantity. According to Mode I fracture, the parameter, ΔW_I is, equations (9) and (10):

$$\Delta W_I = \max_{\theta}\left(\Delta\sigma_n \Delta\varepsilon_n\right) + \left(\Delta\tau\Delta\gamma\right) \quad (9)$$

For Mode II fracture, the parameter, ΔW_{II} is:

$$\Delta W_{II} = \left(\Delta\sigma_n \Delta\varepsilon_n\right) + \max_{\theta}\left(\Delta\tau\Delta\gamma\right) \quad (10)$$

where $\Delta\tau$ and $\Delta\gamma$ are the shear stress range and shear strain range, respectively, $\Delta\sigma_n$ and $\Delta\varepsilon_n$ are the normal stress range and normal strain range, respectively.

4. RESULTS AND DISCUSSIONS

4.1 Experimental cyclic stress-strain behavior under proportional and non-proportional loading

Non-proportional cyclic tests were conducted with the ellipse up (EA) and ellipse down (EB), the rectangle up (RA) and rectangle down (RB), the lozenge up (LA) and lozenge down (LB) loading paths (see Table 3). In Figure 3 is shown the evolution of experimental life with equivalent *von Mises* stress.

Analyzing the results in Figure 3a and Figure 3b and considering the applicability of von Mises criterion, it is shown that loading trajectories exhibit different values of fatigue life for the same von Mises stress, which present the great influence of loading paths in fatigue life and the difficulty of this criterion to estimate the material fatigue life.

The EB and RB cases Figure 3a and Figure 3b, respectively, are the worst loading paths for fatigue life. On the other hand, the EA and RA cases are less harmful to material fatigue life. Thus, it can be seen that the normal component has a greater influence in fatigue life than torsional component. In the middle of the results mentioned before appear the Circle and Square cases. The lozenge cases aren't illustrated here because there isn't available space. Nevertheless, the influence of LA and LB trajectories in fatigue life is very similar to EA, EB and RA, RB trajectories.

As it can be seen in Figure 4, the MCE model collects more results around a central line than *von Mises* criterion. With the application of this model, is not observed a evident distinction between the different loading trajectories. Therefore, with application of MCE model, the results of fatigue life are more independent of the loading path than with *von Mises* criterion. Compared with *von Mises* criterion, MCE model gets better correlations between stress and fatigue life.

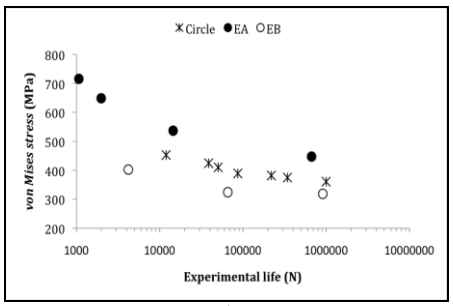

a)

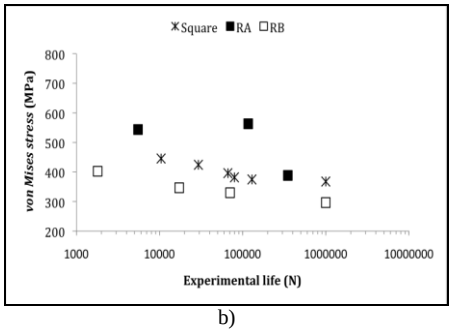

b)

Figure 3 *- Evolution of experimental life with equivalent von Mises stress: a) Circle and Elipse case, b) Square and Rectangle case.*

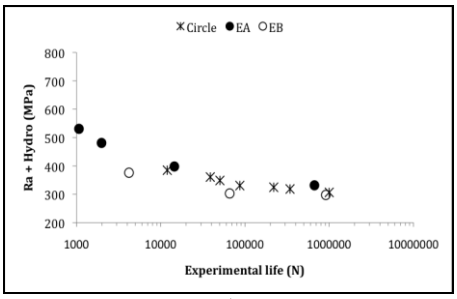

a)

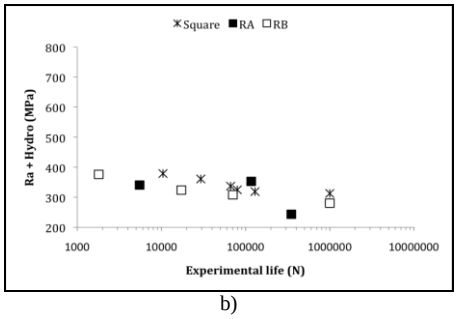

b)

Figure 4 *- Evolution of MCE fatigue parameter with experimental life: a) Circle and Ellipse case, b) Square and Rectangle case.*

4.2 Fractographic analysis of fracture surface and estimation of critical plane orientation

From Figure 5 to Figure 10 it is presented the fractographic analysis of the macroscopic plane of crack initiation.

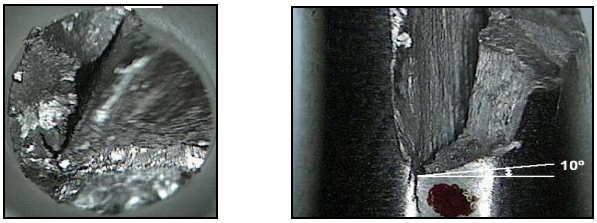

Figure 5 *- Fractographic analysis of the fatigue failure plane orientation under EA loading path shown in Table 3.*

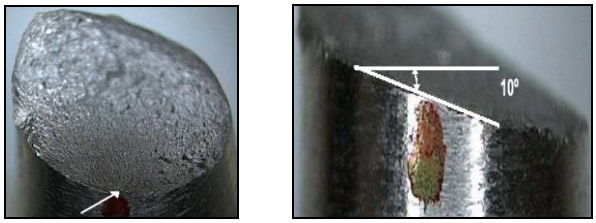

Figure 6 *- Fractographic analysis of the fatigue failure plane orientation under EB loading path shown in Table 3.*

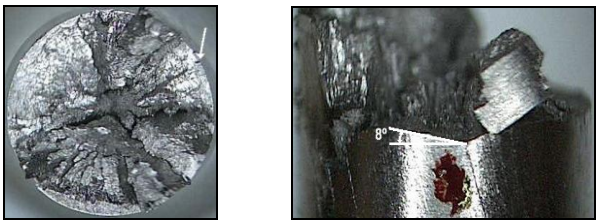

Figure 7 *- Fractographic analysis of the fatigue failure plane orientation under RA loading path shown in Table 3.*

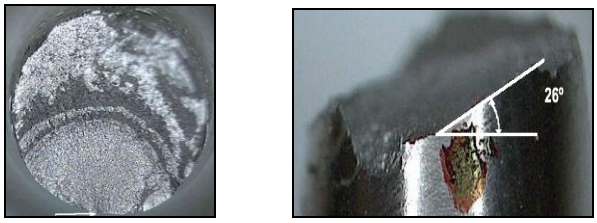

Figure 8 *- Fractographic analysis of the fatigue failure plane orientation under RB loading path shown in Table 3.*

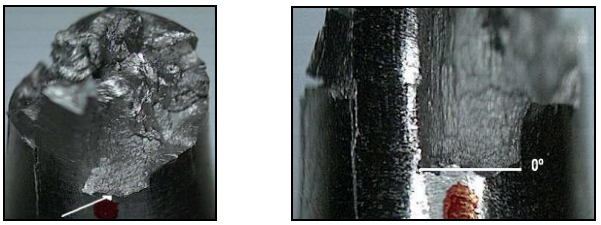

Figure 9 *- Fractographic analysis of the fatigue failure plane orientation under LA loading path shown in Table 3.*

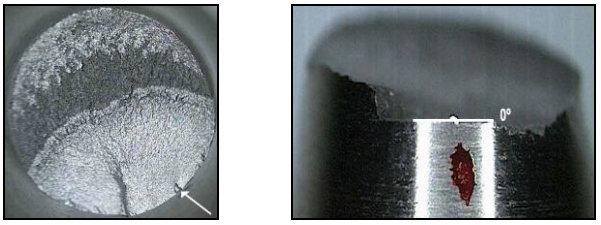

Figure 10 *- Fractographic analysis of the fatigue failure plane orientation under LB loading path shown in Table 3.*

It can be observed that specimens fracture surfaces that were submitted to the down trajectories showed well-defined fatigue typical characteristics. On the other hand, specimens that were submitted to the up trajectories showed fractures surfaces with large cracking and multiple morphologies in the same type of trajectory

4.3 Theoretical analysis of the fatigue crack planes

Critical plane models such as, Findley, Brown-Miller, Fatemi-Socie, S-W-T and Liu criterion, were used to analysed the potential crack plane orientation. Table 5 presents the comparison of the measured crack plane with predictions given by the critical plane models.

Table 5 *- Comparison of the measured crack plane with predictions.*

	Multiaxial Loading Paths								
	Case Circle	Case EA	Case EB	Case Square	Case RA	Case RB	Case Losangle	Case LA	Case LB
Measured	24°	6,5°	6,83°	32°	7,3°	19°	-	7,4°	2°
Findley	0°	0°	±39°	±22°	±9°	±28°	0°	0°	±39°
B-M	0°	0°	±40°	±21°	±7°	±28°	0°	0°	±41°
F-S	0°	0°	±42°	±21°	±7°	±29°	0°	0°	±43°
S-W-T	0°	±38°	0°	±25°	±41°	±15°	0°	±45°	0°
Liu I	0°	±38°	0°	±25°	±41°	±15°	0°	±45°	0°
Liu II	0°/±90°	0°/±90°	±45°	±21°/±69°	±4°/±86°	±30°/±60°	0°/±90°	0°/±90°	±45°

From the results in Table 5, it is easy to observe that the predictions made by the critical plane models depend of the multiaxial fatigue loading paths. The multiaxial fatigue models can be classified as shear-based models (Findley, Brown-Miller, Fatemi-Socie and Liu II) and tensile-based models (SWT and Liu I). Shear-based models give good predictions of the orientation of the crack initiation plane in up loading

cases, Case EA, Case RA and Case LA. Tensile-based models give good predictions of the orientation of the crack initiation plane in down loading cases, Case EB, Case RB and Case LB. The RA and RB cases show the larger difference between measured angles, nearly 12º.

The difference between crack orientation plane in EA and EB cases and Circle case is about 17º. The difference between crack orientation plane in RA and RB cases and Square case is about 25º and 13º respectively. For up loading cases the models that give a better approach for experimental results were *Brown-Miller* and *Fatemi Socie* models; while for down loading cases the models that give a better approach for experimental results were *S-W-T* and *Liu II* models.

5. CONCLUSIONS

A wide range of fatigue loading paths was applied to the austenitic stainless steel *AISI 303*. It was found that the loading paths have significant influences on fatigue life and on the crack plane orientations. Experimental results show that the ratio between normal stress component and shear stress component has a strong influence to fatigue damage and consequently in fatigue life. Down trajectories, with normal component bigger than shear component, have proven to be worse for fatigue life than up trajectories.

The MCE approach gives better correlations than von Mises approach for the studied loading cases and material. The MCE approach also shows that is more independent of the loading case.

The fracture surfaces of the specimens that were submitted to the down trajectories showed well-defined fatigue typical characteristics. Otherwise, specimens that were submitted to the up trajectories showed fractures surfaces with large cracking and multiple morphologies in the same type of trajectory.

Shear-based models give good predictions of the orientation of the crack initiation plane in up loading cases, Case EA, Case RA and Case LA. Tensile-based models give good predictions of the orientation of the crack initiation plane in down loading cases, Case EB, Case RB and Case LB.

ACKNOWLEDGEMENTS

The authors gratefully acknowledge financial support from FCT - Fundação para Ciência e Tecnologia (Portuguese Foundation for Science and Technology), through the project POCTI/EME/59577/2004.

RERERENCES

[1] Susmel, L., Petrone, N. (2003). "Multiaxial Fatigue Life Estimations for 6082-T6 Cylindrical Specimens under In-Phase and Out-of-Phase Biaxial Loadings", Biaxial/Multiaxial Fatigue and Fracture, Editors: A. Carpinteri; M. Freitas; A. Spagnoli, 83-104.

[2] Papadopoulos, I. V. (2001). "Long Life Fatigue under Multiaxial Loading", International Journal of Fatigue 23: 839-849.

[3] Tuthill, A. H. (2002). "Stainless Steels and Specialty Alloys for Modern Pulp and Paper Mills", Reference Book, Series No. 11 025, Nickel Development Institute.

[4] Nickel Institute Web Page (11-10-2008). http://www.nickelinstitute.org/index.cfm/ci_id/11021.htm.

[5] Reis, L., (2004). "Comportamento Mecânico de Aços em Fadiga Multiaxial a Amplitude de Carga Constante e Síncrona", Universidade Técnica de Lisboa, IST, Tese de Doutoramento

[6] Freitas, M., Li, B. e Santos, J. L. T. (2000). "A numerical approach for high-cycle fatigue life prediction with multiaxial loading." Multiaxial Fatigue and Deformation: Testing and Prediction, ASTM STP 1387.

[7] Cruz, A. (2007). "Análise da não Proporcionalidade entre Tensões em Carregamentos Multiaxiais", Universidade Técnica de Lisboa, IST, Tese de Mestrado.

[8] ASTM E606 (2003). "Standard Practice for Strain-Controlled Fatigue Testing - E 606 – 92 (Reapproved 1998)." ASTM 03.01: 1-15.

[9] Socie, D.F. and Marquis, G.B., (2000) Multiaxial Fatigue, SAE, Warrendale, PA.

[10] Shigley, J. E., Mischke, C. R., Budynas, R. G. (2004). "Mechanical Engineering Design", Seventh Edition, Int. Edition, McGraw Hill.

[11] Papadopoulos, I. V., Bernasconi, A., Davoli, P., Filippini, M., Gorla, C. (1997). "A Comparative Study of Multiaxial High Cycle Fatigue Criteria for Metals", International Journal of Fatigue, vol. 19, No. 3, 219-235.

[12] Findley, W. N. (1956). "Theory For Combined Bending And Torsion Fatigue With Data For SAE 4340 Steel", International Conference on Fatigue Metals: 150-157.

[13] Brown, M., Miller, K. J. (1973). "A Theory for Fatigue Failure Under Multiaxial Stress-strain Conditions." Procedings of the Institute of Mechanical Engineers 187: 745-755.

[14] Fatemi, A., Socie, D. (1988). "A Critical Plane Approaches to Multiaxial Fatigue Damage including Out-of-Phase Loading", FFEMS 11(3): 149-165.

[15] Smith, K. N., Watson, P., Topper, T. H. (1970). "A Stress-Strain Function for the Fatigue of Metals", Journal of Materials, JMLSA 5(4): 767-778.

[16] Liu, K. (1993). "A Method Based on Virtual Strain-Energy Parameters for Multiaxial Fatigue Life Prediction", Advances in Multiaxial Fatigue, ASTM STP 1191: 67-84.